A99-33773

AIAA 99–3440

Large-Eddy Simulation of Fuel-Air Mixing and Chemical Reactions in Swirling Flow Combustor

S. Menon W-W. Kim and C. Stone
School of Aerospace Engineering
Georgia Institute of Technology
Atlanta, Georgia 30332
and
B. Sekar
Wright Patterson AFB
Dayton, Ohio 45433

30th Plasmadynamics and Lasers Conference
28 June - July 1, 1999 / Norfolk, VA

Large-Eddy Simulation of Fuel-Air Mixing and Chemical Reactions in Swirling Flow Combustor

S. Menon* W-W. Kim† and C. Stone‡
School of Aerospace Engineering
Georgia Institute of Technology
Atlanta, Georgia 30332
and
B. Sekar§
Wright Patterson AFB
Dayton, Ohio 45433

The ability of large-eddy simulations (LES) to simulate high Reynolds number reacting and non-reacting flows in full-scale combustor configurations is explored in this study. In particular, a generic configuration based on a Dry Low Emission General Electric combustor (LM-6000) is employed to evaluate LES under realistic conditions. Premixed combustion under high swirl conditions is simulated using new flame speed model that accounts for the effect of flame broadening and compared to earlier results and experimental data. Results shows that the inclusion of the flame broadening effect results in a more accurate characterization of the flame structure. The effects of swirl on fuel-air mixing and on a liquid spray dispersion are also studied under realistic conditions in the LM-6000 type of combustor. The computational effort required for these studies suggest that by using higher-order subgrid closure models LES of premixed combustion (using a flame speed model) or fuel-air mixing (even with two-phase) in realistic devices can be completed in a matter of days using currently available massively parallel systems. This demonstration along with the expected speedup of next generation systems establishes the potential of LES for design studies in the near future.

1 Introduction

Time-accurate simulation of turbulent flames in high Reynolds number flows is a challenging task since both fluid dynamics and combustion must be modeled and/or resolved accurately. Direct simulations (in which all scales are resolved and no models are used) are not practical since the grid resolution and the computational resource requirements far exceed the computational capability available at present and possibly in the near future. On the other hand, Reynolds-Averaged methods are not acceptable since they predict the mean motion using a global model for all turbulent scales and ignore the unsteady dynamics (which is critical for accurate predictions). In the present study, we explore the ability of large-eddy simulations (LES) for simulating high Reynolds number reacting and non-reacting flows in realistic full-scale combustor configurations.

The underlying philosophy behind LES is to explicitly calculate the large energy-containing scales of motion which are directly affected by boundary conditions while modeling only the small scales of the flow. The large scales are difficult to model due to their variability from one problem geometry to the next. The smaller scales are presumed to be more universal in nature and therefore, more amenable to modeling. The LES equations of motion describe the evolution of only the large scales and are derived by applying a *spatial* filter function to the conservation equations. The effect of the unresolved small scales appear as additional subgrid terms in the large-scale or resolved field equations. These terms must be modeled or additional equations for these terms derived in order to close the LES equations. Since only the small scales are modeled it has been suggested that this approach can be used to study relatively high Reynolds number flows. However, most LES applications reported in the past have been limited

*Professor, AIAA Senior Member
†Post-Doctoral Fellow, AIAA Member
‡Graduate Research Assistant, AIAA Student Member
§AIAA Member

to simple and/or relatively low Reynolds number flows. The present study employs LES to study turbulent premixed combustion, non-premixed fuel-air mixing and spray dispersion in complex flows under conditions typical of full-scale devices. To successfully accomplish such simulations new methodologies need to be integrated and demonstrated. The present study addresses some of these issues within the 'practical' constraint that for engineering applications, such simulations need to be completed in a matter of days without significantly compromising the accuracy of the predictions.

A combustor that (in terms of dimensions and flow conditions) is part of a Dry Low Emission (DLE) LM-6000 lean premixed combustor being developed by General Electric Aircraft Engine (GEAE) Company is employed for the present study. In the LM 6000, the mixing is caused by a dual, annular counter-rotating swirler premixer and the premixed mixture enters the combustor either in a fully premixed or in a partially premixed state. When the mixture is fully premixed, under certain conditions (i.e., appropriate Reynolds and Damkohler numbers) the flame is very thin and flamelet models can be used effectively and quite accurately, as demonstrated earlier.[1] In the present study, premixed combustion in the LM-6000 is repeated using an improved thin flame model that includes the effect of flame broadening.

Although fully premixing may be preferred recent experiments using a similar setup[2] indicate that there is a significant spatial and temporal variation in the fuel-air mixedness in the combustor. For example, data showed a maximum spatial variation on the order of 50% of the known overall equivalence ratio and a temporal unmixedness in peak equivalence ratio 2.4 times larger than the overall stoichiometry. This spatio-temporal variation in the mixedness is very important to quantify from design standpoint since variation in the local equivalence ratio can adversely impact NOx emission levels[3] and, especially in the lean case, result in combustion instability.[4]

To determine if this unmixedness can be numerically predicted, the experimental configuration[2] is also simulated here. However, for LES of scalar mixing some fundamentally different issues need to be considered. Stirring by the turbulent eddies must be accompanied by molecular diffusion to achieve mixing of species. Both these features must be modeled or simulated accurately to predict local mixedness. However, in conventional LES when eddy-diffusivity closure (using arguments analogous to those used for the closure of the subgrid stresses based on eddy viscosity) is employed, then it is implicitly assumed that both small-scale turbulent stirring *and* molecular diffusion can be modeled using an effective eddy diffusivity that scales with the subgrid eddy viscosity (using a turbulent Schmidt number). In general, this assumption is obviously not justifiable but it has not yet been established what are the quantifiable errors inherent in this approach when employed to study engineering flows of interest, especially when only fuel-air unsteady mixing at very high Reynolds number is of interest. This issue is addressed in the present study.

Note that flows with realistic heat release enforce additional constraints that may not be adequately captured by an eddy diffusivity subgrid closure. This is because the final stage of mixing is critical for accurate prediction of the heat release effect (which in turn impacts the flow field via volumetric expansion). Therefore, it is of interest to determine if conventional closure can be utilized (with verifiable estimate of error) for engineering design studies. Failure of this type of closure would indicate the need for (and, in fact demand) a subgrid scalar closure that accounts for both small-scale turbulent stirring and molecular diffusion processes more accurately.[5-7]

Another issue of interest is to evaluate the ability of LES to deal with two-phase flows since, in most practical combustors, fuel is introduced in liquid form and spray vaporization and gaseous mixing must occur prior to the combustion process. Recently, a new two-phase LES methodology was developed to simulate spray combustion in full-scale devices.[8] This capability is also utilized here to investigate droplet dispersion in the LM6000 configuration.

In summary, this paper addresses some of the issues involved in carrying out LES of high Reynolds number flows using test and flow conditions that are representative of full-scale devices. The ability of the subgrid closure within the constraints of a coarse grid resolution and a computational turnaround time acceptable from engineering standpoint is particularly addressed in this paper. Note that to achieve efficient computations, the LES solver has to be implemented in massively parallel systems and the parallel algorithm must be efficient and scalable. Otherwise, the computational cost for such studies will still be unacceptable.

2 The Simulation Model

The LES equations are derived from the compressible Navier Stokes equations for multi-species,

reacting fluid by Favre-filtering.[9] Thus,

$$\begin{aligned}
&\frac{\partial \bar{\rho}}{\partial t} + \frac{\partial \bar{\rho}\widetilde{u_i}}{\partial x_i} = 0 \\
&\frac{\partial \bar{\rho}\widetilde{u_i}}{\partial t} + \frac{\partial}{\partial x_j}[\bar{\rho}\widetilde{u_i}\widetilde{u_j} + \bar{p}\delta_{ij} - \overline{\tau}_{ij} + \tau_{ij}^{sgs}] = F_p \\
&\frac{\partial \bar{\rho}\widetilde{E}}{\partial t} + \frac{\partial}{\partial x_i}[(\bar{\rho}\widetilde{E} + \bar{p})\widetilde{u}_i + \bar{q}_i - \widetilde{u}_j\overline{\tau}_{ij} \\
&+ H_i^{sgs} + \sigma_{ij}^{sgs} + E_p] = 0 \\
&\frac{\partial \bar{\rho}\tilde{Y}_m}{\partial t} + \frac{\partial}{\partial x_i}[\bar{\rho}\tilde{Y}_m\tilde{u}_i - \bar{\rho}\tilde{D}_m\frac{\partial \tilde{Y}_m}{\partial x_i} + \Phi_{i,m}^{sgs} + \theta_{i,m}^{sgs}] = \overline{\dot{w}}_m
\end{aligned} \tag{1}$$

Here, over bar and $\sim$ denotes the resolved filtered variables. Also, ρ is the mass density, p is the pressure, E is the total energy per unit mass, u_i is the velocity vector, q_i is the heat flux vector, and τ_{ij} is the viscous stress tensor. The individual species mass fraction, diffusion velocities, and mass reaction rate per unit volume are, respectively, Y_m, $V_{i,m}$, and $\dot{w}_m$. The viscous stress tensor is $\tau_{ij} = \mu(\partial u_i/\partial x_j + \partial u_j/\partial x_i) - \frac{2}{3}\mu(\partial u_k/\partial x_k)\delta_{ij}$ where μ is the molecular viscosity coefficient approximated using Sutherland's Law. The diffusion velocities are approximated by Fick's law: $V_{i,m} = (-D_m/Y_m)(\partial Y_m/\partial x_i)$ where D_m is the mixture averaged molecular diffusion coefficient. Here, $\overline{\tau}_{ij}$ and $\overline{q}_i$ are approximated in terms of the filtered velocity. Finally, pressure is determined from the filtered equation of state for a perfect gas mixture. Further details are given elsewhere and therefore, avoided for brevity.

The unclosed subgrid terms representing respectively, the subgrid stress tensor, subgrid heat flux, unresolved viscous work, species mass flux, diffusive mass flux, and filtered reaction rate are:

$$\begin{aligned}
&\tau_{ij}^{sgs} = \bar{\rho}[\widetilde{u_iu_j} - \widetilde{u}_i\widetilde{u}_j] \\
&H_i^{sgs} = \bar{\rho}[\widetilde{Eu_i} - \widetilde{E}\widetilde{u}_i] + [\overline{pu_i} - \bar{p}\widetilde{u}_i] \\
&\sigma_i^{sgs} = [\overline{u_j\tau_{ij}} - \widetilde{u}_j\overline{\tau}_{ij}] \\
&\Phi_{i,m}^{sgs} = \bar{\rho}[\widetilde{u_iY_m} - \tilde{u}_i\tilde{Y}_m] \\
&\theta_{i,m}^{sgs} = \bar{\rho}[\widetilde{V_{i,m}Y_m} - \tilde{V}_{i,m}\tilde{Y}_m] \\
&\overline{\dot{w}}_m
\end{aligned} \tag{2}$$

All these terms have to be specified to close the LES equations given above. The closure models are briefly discussed in the next section.

In the above equations, the terms F_p and E_p are respectively, the force due to particles in the momentum and the work done by the force in the energy equation. These terms are given elsewhere[10] and therefore, avoided here for brevity.

To track the particles within the gas field a Stochastic Separated Flow (SSF) Lagrangian formulation[11,12] is used. Essentially, the equation of motion of each droplet group is solved in the Lagrangian co-ordinate system within the Eulerian gas phase LES flow field. The gas phase velocity field used in the particle equations of motion is obtained using both the filtered LES velocity field and the subgrid kinetic energy.[10,13] This approach includes the stochastic turbulent dispersion effect into the formulation (via the subgrid kinetic energy). Note that this effect cannot be included when an algebraic eddy viscosity (e.g., Smagorinsky type) is used. Again, details are reported the cited references and therefore, avoided here.

3 Subgrid Closure

The closure of the subgrid terms is achieved in this study using a localized dynamic eddy-viscosity/diffusivity model. A summary of this closure is given here.

3.1 Momentum and Energy Transport Closure

A compressible version of the localized dynamic model introduced earlier[14] is employed. The subgrid eddy viscosity in this model is determined by using the grid size Δ as the characteristic length scale and the subgrid kinetic energy as the characteristic velocity scale. The subgrid kinetic energy is defined as $k^{sgs} = \frac{1}{2}[\widetilde{u_k^2} - \widetilde{u}_k^2]$ and is obtained by solving the following transport equation [15,]:

$$\frac{\partial \bar{\rho}k^{sgs}}{\partial t} + \frac{\partial}{\partial x_i}(\bar{\rho}\widetilde{u}_ik^{sgs}) = P^{sgs} - D^{sgs} + \frac{\partial}{\partial x_i}\left(\frac{\bar{\rho}\nu_t}{Pr_t}\frac{\partial k^{sgs}}{\partial x_i}\right) F_k \tag{3}$$

Here, Pr_t is the turbulent Prandtl number. The terms on the right side of equation (3) represent, respectively, the production, the dissipation, the transport and the work done by droplets (in case of two-phase flows) of the subgrid kinetic energy. The production term is $P^{sgs} = -\tau_{ij}^{sgs}(\partial\widetilde{u}_i/\partial x_j)$ and the subgrid shear stresses τ_{ij}^{sgs} are obtained from the relation:

$$\tau_{ij}^{sgs} = -2\bar{\rho}\nu_t(\widetilde{S}_{ij} - \frac{1}{3}\widetilde{S}_{kk}\delta_{ij}) + \frac{2}{3}\bar{\rho}k^{sgs}\delta_{ij}. \tag{4}$$

Here, ν_t is the subgrid eddy viscosity given by $\nu_t = C_\nu(k^{sgs})^{1/2}\overline{\Delta}$ and $\widetilde{S}_{ij} = \frac{1}{2}(\partial\widetilde{u}_i/\partial x_j + \partial\widetilde{u}_j/\partial x_i)$ is the resolved-scale rate-of-strain tensor. Finally, the dissipation term is modeled as $D^{sgs} = C_\varepsilon\bar{\rho}(k^{sgs})^{3/2}/\overline{\Delta}$.

The two coefficients appearing in the above equations, C_ν and C_ε, are determined dynamically and locally (in space and time) using the k-equation subgrid model. The details of this model is given elsewhere[16] and therefore, only key relevant issues are noted here. For example, in two-phase flows an additional term due to the force term F_p (in the momentum equation) appears in the k-equation (i.e. F_k) that needs to be modeled. The present study neglects this term but another study is addressing this issue.

As in other dynamic model,[17] the present k-equation model also assumes scale similarity in the inertial subrange. This implies that the stresses at the cutoff (i.e., the grid size, $\overline{\Delta}$) can be related to stresses at twice the cutoff (i.e., the test-filter width, ($\widehat{\Delta} = 2\overline{\Delta}$) provided that both these scales are resolved. It has been demonstrated that the present dynamic closure can be formulated without encountering some of the mathematical inconsistencies of Germano *et al.*'s dynamic formulation. These mathematical inconsistencies have been discussed extensively in the literature.[18] Furthermore, the prolonged existence of a negative eddy viscosity[19] for the algebraic model can be avoided here since the subgrid kinetic energy never becomes negative (k^{sgs} also naturally becomes zero in laminar and near-wall regions). Moreover, the coefficient C_ϵ determined using the present approach does not vanish in the limit of high Reynolds number unlike the phenomenon observed in an earlier dynamic kinetic energy model formulation.[20]

From a computational standpoint, the cost of the present dynamic procedure is only slightly more than the Germano *et al.*'s dynamic model due to the additional equation for k^{sgs}. The accuracy of one-equation eddy-viscosity model in reacting flows was recently discussed.[21] As noted elsewhere, in LES using very high grid resolution the effects of the subgrid model on the statistical quantities are usually marginal and both algebraic and one-equation models are equally applicable. However, when a coarse grid is employed (as in the present study) non-equilibrium between subgrid kinetic energy production and dissipation will occur and must be allowed. This is only possible when the one-equation model is employed as recently demonstrated.[16] Interestingly, the superior ability of the present model was also confirmed in an independent study.[22]

3.2 Scalar Transport Closure

For non-reacting fuel-air mixing (of interest here) only the terms $\Phi_{i,m}^{sgs}$ and $\theta_{i,m}^{sgs}$ need to be determined. A conventional closure for the subgrid scalar-velocity correlations $\Phi_{i,m}^{sgs}$ is

$$\Phi_{i,m}^{sgs} = -\bar{\rho}\frac{\nu_T}{Sc_t}\frac{\partial \tilde{Y}_m}{\partial x_i} \qquad (5)$$

where Sc_t is the turbulent Schmidt number (although Sc_t can be determined using a dynamic model, here $Sc_t = 1$ is assumed for simplicity).

The magnitude of $\Phi_{i,m}^{sgs}$, as modeled in equation (5), is expected to dominate the diffusive mass flux term $\theta_{i,m}^{sgs}$ (which represents the effect of molecular diffusion in the filtered species equation) in high Reynolds numbers flows when the subgrid turbulent kinetic energy is large. When $\Phi_{i,m}^{sgs}$ swamps $\theta_{i,m}^{sgs}$, the final solution can be expected to be invariant with the molecular diffusion process. This was found to be the case in a recent study[1] of high Reynolds number jet flows modeled using equation (5). Since a similar high-Re swirling jet flow is considered here $\theta_{i,m}^{sgs}$ is neglected from the resolved-scale equation.

It is emphasized that the present study is evaluating a first-level approximation for scalar mixing for high-Re LES of engineering flows. As such, some over-reaching approximations and (possibly questionable) assumptions are invoked in the model formulation (such as a gradient diffusion approximation in Eq. 5). It is well understood that this approach may not be accurate or even applicable in reacting flows due to the importance of molecular diffusion at the small scales (ignored in the present model) even in high-Re flows. Past studies have already indicated the failure of eddy diffusivity gradient diffusion models in reacting flows.[23] An alternative modeling approach which explicitly incorporates both turbulent stirring and molecular diffusion within the subgrid closure has been developed recently.[5-7,24] However, the increased computational cost of this approach may not be warranted from engineering non-reacting flow studies if the more simpler eddy diffusivity model can be used with reasonable accuracy.

Another approach currently being investigated[25] involves simulating the subgrid evolution of the joint scalar-velocity correlations such that the correlation $\Phi_{i,m}^{sgs}$ is directly simulated within the subgrid. This approach avoids using the standard gradient-diffusivity model. Preliminary results reported recently[25] shows that this approach has significant potential but still needs further development.

3.3 Premixed Flame Speed Closure

The conventional flame speed model is based on a thin-flame model. A scalar (G) field in a fluid that self-propagates at speed S_L is used to model the flame. The equation governing this G equation on Favre-LES filtering leads to the following equation.[26]

$$\frac{\partial(\bar{\rho}\tilde{G})}{\partial t}+\frac{\partial(\bar{\rho}\tilde{G}\tilde{u}_j)}{\partial x_j} = -\overline{\rho_o S_L^o|\nabla G|}-\frac{\partial}{\partial x_j}\left[\bar{\rho}(\widetilde{u_j G}-\tilde{u}_j\tilde{G})\right] \qquad (6)$$

Here, ρ_o is the reference density and S_L^o is the laminar flame corresponding to this value of density. The source term in the above equation, which includes the effect of subgrid turbulence (wrinkling due to subgrid eddies) is modeled using a flame speed model such that as: $\overline{\rho_o S_L^o|\nabla G|} = \rho_o u_f|\nabla\tilde{G}|$.

Here, u_f is given in terms of the turbulent intensity u' (which can be estimated using k^{sgs}) and S_L. Various models have been proposed for u_f, for example, the Yakhot's model[27] and the Pocheau's model.[28] We will discuss these models here. The second term on the right hand side of the above equation represents the unresolved transport (due to subgrid velocity field) and is customarily modeled using a gradient diffusion assumption[29]

A key development recently was the inclusion of the flame broadening effect on u_f as reported recently.[30] For example, the flame speed in the above equation, S_L is the un-stretched laminar speed and is strictly applicable in the thin flame limit. However, if the turbulent scale smaller than the flame thickness exist in the flow then these scales will modify the flame structure. A major effect is a broadened flame[31] with a characteristic thickness larger than the laminar flame thickness. As a result, the the laminar flame speed will also be different. Analogous to the thin flames, the broadened flame will be wrinkled by turbulent fluctuations at scales larger than the broadened flame thickness.

In the present effort, a flame-broadened model has been incorporated in order to simulate flows at conditions that cannot be investigated using the classical thin flame model. As shown later, this approach results in an improved prediction of the flame structure as well as in a more accurate estimate of the turbulence behavior. The actual formulation is too extensive to be reported here but is described in a recent paper.[30]

3.4 Two-phase Subgrid Closure

The subgrid closure discussed above was primarily developed for gas phase combustion. To deal with two-phase combustion in a similar manner additional models have to be incorporated. Earlier studies[10,13,32] have discussed a new methodology that takes into account the physics of spray transport and mixing. As noted earlier, in a typical LES formulation of two-phase mixing and combustion the droplets are tracked using the Lagrangian formulation only up to a pre-specified cut off size. Beyond this cut-off the droplets are assumed to instantaneously evaporate and mix with the oxidizer. Although this choice of the cutoff size is determined by computational constraints, the somewhat arbitrary choice can have serious impact on the accuracy of the predictions. A new methodology to deal with this effect has been developed as reported earlier.[8] In the present study, only non-vaporizing droplet transport and dispersion in a highly swirling flow is simulated. Momentum coupling included in the present formulation allows for the stochastic dispersion of the droplets by using the subgrid kinetics energy (in addition to the resolved velocity) in the momentum term. Again, details are in cited references.

4 Numerical Approach

In this section we discuss the various issues related to the numerical implementation of the LES models for the problems of interest.

4.1 Configurations and Test Conditions

The computational domain for the GEAE LM-6000 combustor is the region downstream of the dual annular counter-rotating swirler premixer.[33] Two configurations are studied here. The first one is a combustor that has been studied experimentally at GE and is shown schematically in figure 1. Premixed combustion and spray dispersion in this configuration are studied in this combustor.

Another configuration very similar to LM-6000 is a combustor being studied at University of Illinois, Urbana-Champaign. A centerline sectional view of this combustor is shown in figure 2. Also shown are the locations where experimental data (primarily histograms) was obtained. The premixer exit (i.e., combustor inlet) diameter is 48mm and the combustor diameter is 129mm. Therefore, the increase in the cross-sectional area over the backward facing step of the dump combustor is 7.2:1 which is quite large. In addition to the dimensions the key difference between LM-6000 model at GE and the UIUC combustor is that the latter has a circular cross-section (and is more representative of the flight hardware).

In both the combustors, a swirling jet (the maximum value of tangential velocity component is slightly greater than the peak value of axial velocity component) is injected from the premixer at a pressure of 1.16×10^5 N/m^2. The swirl number $S = \int_0^R \rho u w r^2 dr / R \int_0^R \rho u^2 r dr$ was about 0.56 which belongs to the regime where onset of an internal recirculation zone (IRZ) occurs.[34] The radial number $R = \int_0^R \rho u v r dr / \int_0^R \rho u^2 r dr$ which represents the effect of inlet radial velocity is 0.012 for the present case. The Reynolds number Re based on the inlet mean streamwise velocity and the inlet jet diameter D_0 is 330,000.

4.2 Computational Cost

The computational domain is resolved in this study using a resolution of $101 \times 61 \times 81$ grid points along, the axial, the radial, and the azimuthal directions, respectively. The grid was clustered in regions

of interest (such as the jet shear layer). However, it should be obvious that the chosen grid is very coarse for the Reynolds number of the flow. Therefore, these LES must be considered 'engineering' LES with the primary goal to determine if such a coarse grid LES is capable of providing an accurate representation of the global variables of interest to the engine manufacturers.

Even with such a coarse grid the computational cost can be significant. This is primarily due to the need to simulate the flowfield in a time-accurate manner and for analysis sufficient data must be recorded for statistical analysis; typically 10 flow through times. The computational cost on the Cray T3E using the grid noted above, 2 GB of run-time memory and 600-1000 single processor hours are needed to obtain a single flow through time (defined as the approximate time for the flow to go from the inlet to the exit).

Real time for such simulations depend on system availability. Using 120-processors, it was possible to get one flow-through time within 6 (real time) hours. Thus, provided 120 processors were available a complete simulation (or around 10 flow-through times) can be accomplished in 2.5 days (assuming full-time availability) Although this appears to be quite extensive (and idealistic since full-time availability is impossible) it is worth noting that the continuing increase in computational speed (accompanied by drastic reduction in the cost) and the scalability of the MPI based code used here suggest that such simulations may be feasible in 1-2 days on next generation systems (perhaps on PC - Intel PC clusters).

4.3 Numerical Scheme

The numerical algorithm solves the full, unsteady, compressible Navier-Stokes equations (and the k^sgs equation) using a finite-volume code that is fourth-order accurate in space and second-order accurate in time. The initial conditions were set approximately using turbulent jet profiles and, therefore, a period of time was required to wash out the effect of the initial conditions out before accurate data can be collected. The inflow conditions at the premixer exit were specified based on the information provided by GEAE for both the LM-6000 premixed combustion and UIUC fuel-air mixing cases. An inflow turbulent field was generated by using a specified turbulence intensity profile (with an intensity of 7%) on randomly generated Gaussian velocity fields. More details are given elsewhere.[1]

For the fuel-air mixing case in the UIUC combustor, the inflow equivalence ratio profile was available from data. The profile indicates a fuel-rich annulus emanating from the outer regions of the premixer exit. Based on this inlet equivalence ratio profile, the inlet fuel-species mass fraction (Y_F) distribution are prescribed: $Y_F = \Phi/(\Phi + (A/F)_{stoic})$ where $(A/F)_{stoic}$ is the stoichiometric air-fuel ratio. In the present study, methane (CH_4) fuel is used and therefore, $(A/F)_{stoic}$=17.12. Unfortunately, it was quite difficult to fully incorporate and resolve the fluctuation in the equivalence ratio observed in the experiments using the present grid resolution (about 24 grid cells were used to resolve one-half of the inlet diameter). Therefore, a compromise was made whereby the inlet profile used for LES was a smoothened version of the measured profile, as discussed earlier[34]

At the combustor exit, characteristic outflow boundary conditions[35] were imposed. To prevent reverse flow (which will adversely affect the characteristic outflow boundary conditions) from appearing near the outflow, a buffer region was added and its area was linearly contracted by 25% (this buffer extension at the exit is shown in Figure 1(b)). For reacting cases, the effect of the contraction on the time-averaged LES predictions was negligible as demonstrated by Kim *et al.*[1] To obtain statistically stationary results for comparison with the PLIF data the LES results were time-averaged for over 10 flow-through times based on the mean centerline axial velocity at the inlet after an initial relaxation time of around 5 flow through times. Ensemble average along the homogeneous azimuthal direction was also carried out when required.

5 Results and Discussion

The results for both premixed and non-premixed combustion in the LM-6000 type combustor is summarized here.

5.1 Premixed combustion in LM-6000

As noted above, earlier studies using a thin flame model based on the G equation gave very good agreement with experimental data.[1] However, in that study the flame speed model was based on a fit to the experimental data using a model proposed earlier[28] of the form: $u_f/S_L = (1 + \beta u'^{\gamma})$ where u_f is the turbulent flame speed, u' is the turbulence intensity (obtained using the subgrid kinetic energy), β is an adjustable parameter and $\gamma = 2$ to conserve energy. The earlier study also demonstrated that for the test conditions of the LM-6000 the analytical flame speed model obtained using RNG[27] $u_f/S_L = exp[(u'/S_L)^2]$ severely under predicted the flame speed. This was disappointing since Yakhot's model had no adjustable constants (such as

β in the Pocheau's model) and therefore, could be used in different flows without requiring calibration. The recent study[30] has shown that the new flame-broadened model allows us to use both Yakhot's and Pocheau's model to obtain good accuracy in the results. Some of these results are summarized here to highlight this new capability.

Figure 3 shows a typical snapshot of the flame structure as predicted by the flame-broadened Yakhot's model coupled with the dynamic evaluation of the G-equation. As can be seen the flame structure is highly wrinkled and regions with cusps are present. These features are in qualitative agreement with data. A similar result was obtained using Pocheau's model.[30]

Various test models were studied earlier.[30] Here, we present some results obtained using the Pocheau's model. Three models are compared in the following figures: PTC20, PTD20 and PBD20. The first letter indicates Pocheau's turbulent flame speed model is employed, the second letter indicates either the broadened-flame model ("B") or the conventional thin flame model ("T"). In the conventional thin flame model, a maximum value of u'/S_L is prescribed to prevent overestimation of turbulent flame speed at high u'/S_L. Above this maximum u'/S_L, turbulent flame speed is assumed to be constant. Following earlier studies,[7] the maximum u'/S_L is set to be 20 for Yakhot's model and 16.6 for Pocheau's model. The third letter indicates if the dynamic model (to determine the turbulent Schmidt number Sc^G is employed. If the dynamic model is used, the letter will be "D". Otherwise, it will be "C" which stands for constant turbulent Schmidt number. The number in the last place indicates the value of the adjustable parameter β in Pocheau's model. Various values of β (i.e., 2, 10, 20, and 30) were tested. These values were chosen based on our earlier study[34] where β was calibrated using the experiment[36] of stabilized turbulent premixed flames by a weak swirl or by a stagnation plate. It was observed that $\beta = 20$ case compares well with the experiment.

The Reynolds number is high enough that fully developed turbulence can be assumed. Observations suggest that the ratio u'/S_L can be locally as large as 100's in this combustor. Using non-dimensional parameters to characterize flame-turbulence interactions, several regimes of interest can be identified.[37] Typically, Re, Da, and Ka are used for this purpose. Here, $Re = u'\ell/\nu$ (where ℓ is the integral length scale, approximated here by the inlet jet diameter D_0), $Da = \tau_t/\tau_c$ is the Damköhler number (which is defined as a ratio of a characteristic flow time τ_t to a characteristic chemical reaction time τ_c), and $Ka = (\delta_L/S_L A)\, dA/dt$ (where $(1/A)\, dA/dt$ is the incremental change in flame surface area due to flame stretch) is the turbulent Karlovitz number which is defined to provide a measure of flame stretch. In the present case, $Re = 110,000$, $Da = 8$, and $Ka = 42$. According to Peters[38] the present problem belongs to the thin reaction zone regime. This problem, therefore, is a good test case to validate the broadened-flame model.

Figures 4a and 4b show respectively, the mean axial velocity variation along the centerline and the mean tangential (swirl) velocity variation at a fixed axial location. Both the LES (using the three models) and the experimental data are shown. Note that, hereafter, all velocity components (both mean and turbulence intensity) and the coordinates are nondimensionalized, respectively, using the maximum mean axial velocity at the inlet (U_0) and the inlet jet diameter (D_0). The conventional Pocheau's model based on the thin flame model (PTC20 and PTD20) predicts significantly higher axial velocity after the flame location at $x/D_0 = 0.81$. Again, no significant difference is found between the test models PTC20 and PTD20. Pocheau's model when combined with the broadened-flame model (PBD20) predicts the mean axial velocity variation most accurately in comparison with the experiment. Different values of β do not significantly change this agreement as shown in Fig. 3(c). However, $\beta = 20$ is the only case which does not result in the noticeable centerline recirculation zone and, therfore, shows the best agreement with the experimental data.

Figure 4b shows the nondimensionalized mean tangential (i.e., swirl) velocity (V) profiles in the z-direction at the downstream location, $x/D_0 = 0.18$. All the test models result in more distinguished peaks than the experimental data. Broadened-flame versions of Yakhot's model (YBC and YBD) and Pocheau's model with $\beta = 20$ (PBD20) all show improved prediction in the entire range including the near wall region.

Figures 5a and 5b show respectively, the nondimensionalized mean radial velocity (W) profiles in the y-direction at $x/D_0 = 0.18$ and at $x/D_0 = 0.72$. In this comparison, most of the models behave similarly and predict the experimental data reasonably well. Only the broadened-flame versions of Pocheau's model show the smooth variation of mean radial velocity profiles in the range of $-0.8 < y/D_0 < 0.8$ as is observed in the experimental data. The other models show some fluctuations in this range (not shown).

Figures 6a and 6b show respectively, the root-

mean-square (RMS) profiles of the fluctuating axial velocity components (u_{rms}) along the centerline of the combustor and another off-center location. The broadened-flame versions of Pocheau's model clearly predict the experimental data better than the thin flame model. The disagreement is primarily due to the problems with specifying the inflow turbulence. Realistic turbulence is not fed into the computational domain and, thus, for a small region turbulence has to evolve realistically. Due to this, the turbulence intensity predicted by all the LES initially drops near the inlet while the experimental data tends to remain finite there. However, since swirling jet flows are usually very unstable, realistic turbulent flow is believed to be triggered quickly near the inlet.

Since the discrepancy between the experimental data and the LES results is due to the non-physical turbulence at the inlet, it is expected that the experiment and the LES become more comparable in the locations where inlet condition effects are not significant. Figure 6b shows one example of such locations. This plot presents the x-directional (i.e., streamwise directional) variation of u_{rms} in the corner of the combustor, $y/D_0 = z/D_0 = 0.81$. (Note that the origin of the coordinates is the centerline point at the inlet. This y and z location,therefore, is outside the combustor inlet.) All the LES results shows an reasonable agreement with the experimental data.

Finally, figures 7a and 7b show respectively, the y-directional variation of u_{rms} at $x/D_0 = 0.18$ and the radial velocity fluctuations at $x/D_0 = 0.72$. Again, the broadened-flame version of Pocheau's model shows a better comparison than the other test models especially near centerline region (i.e., $-0.4 < y/D_0 < 0.4$).

The other two fluctuating components show similar agreement with the experiment at this x location and at further downstream locations. For example, in 7b the broadened-flame version of Pocheau's model show reasonable comparison with the experiment.

5.2 Fuel-Air Mixing in LM-6000

As noted above, the premixer of the LM-6000 is designed to fully premix the fuel and the oxidizer. However, in reality the mixing process can be inefficient such that there can be significant variance in the equivalence ratio of the mixture entering the combustor. In this case, premixed combustion modeling using the G-equation is not possible and scalar diffusion mixing between the two species must be modeled. To investigate the ability of a conventional closure to capture the mixing process, a series of calculations were carried out using test data from the experiments at UIUC.

An instantaneous and the time-averaged flow field in the combustor for the fuel-air mixing case are shown in figure 8. As can be clearly seen there are many unsteady features in the flow that evolve with time; however, time averaging washes out all these finer details. Note that the unsteady data was time-averaged to obtain the steady picture and is not a prediction by RANS type of solver. This study emphasizes the need for analysis of the time-dependent flow fields directly.

Figure 9 compares the the point histogram of equivalence ratio measured by Frazier *et al.*[2] and the present LES results. The experimental histogram used only 60 samples at each location to obtain this result which is insufficient to obtain statistically stationary data (additional experiments are underway to obtain additional samples but this data is currently unavailable). On the other hand, the LES histograms are computed using 12000 samples at each location and is considered to have reached statistical stationary state. Therefore, the peaks of the histogram (number of counts) are not expected to be similar and only the extent of variation in the equivalence ratio can be compared. As mentioned earlier, pockets containing fuel-rich mixtures emanate from the outer regions of the premixer exit. The broad equivalence ratio distributions of the point histogram along the edge of the premixer exit (location "d") exemplify the fluctuating nature of these pockets. Flow reversal and turbulent mixing was sufficient to produce a uniform mixture concentration in the recirculation regions near the premixer exit surface corner (location "g"). LES results show that this uniform mixture concentration persists at the downstream locations while the histograms from the experiment were broadened. This discrepancy needs to be revisited when additional experimental data becomes available for more reliable estimates. It is however, worth noting that in spite of this difference there is a reasonable agreement between experimental and LES data.

5.3 Turbulent spray dispersion in LM-6000

The above studies were carried out using the full compressible LES code in order to mimic actual test geometries (which are confined configurations where vortex-acoustic coupling is going to occur especially in reacting flows). However, when acoustic coupling is not important a more efficient a zero-Mach number code developed earlier[8,39] can be used. Here, we use this code to investigate the dispersion of a swirling liquid fuel spray in a high Reynolds number

flow under conditions identical to the case studied for premixed combustion using the compressible code. Momentum coupling between the two phases was included to allow for the relative motion of the fluid and liquid particles.

A very high resolution grid of 201x135x93 was used and approximately 65000 particle trajectories were simulated in this study. Such a resolution has never been attempted in the past and the present study provides an unique opportunity to investigate the physics of spray dispersion. For this application, the code typically takes around 600 single-processor hours on the SGI Origin 2000 for a flow through time and therefore, a typical simulation of 10 flow through times requires around 6000 single processor hours (which is substantially lower than for the compressible case using the same grid and particle resolution). This study is still underway; however, some preliminary results are described below to demonstrate the capability that is now available.

Figure 10 show the vorticity contours and droplet pattern at three axial locations. Here, D is the diameter of the inlet duct. As can be seen in these figures in the plane very close to the inlet the swirling spray follows very closely the swirling shear layer. Note that particles are also seen in regions further away from the shear layer. This is partly due to the recirculation in the dump region and also due to the fact that smaller droplets traverses further away from the shear region. However, further downstream the particles are well dispersed due to the high swirl and there is not much of correlation between the shear regions in the jet flow and the droplet locations. Closer observation of the droplet pattern shows that the droplets tend to cluster in region of low vorticity such as in the braid regions or in-between the vortex tubes formed by the swirl. This observation is in good agreement with experimental observation. Further analysis of the particle dispersion in the shear region and in the combustor is underway and will be reported in the near future.

Finally, 11 shows the particle number density and the Sauter Mean Diameter (SMD) distribution in the radial direction at various axial locations. This data is not fully time-averaged (simulation is still underway) but does provide some interesting insights into the particle dispersion process in high swirl. It can be seen that the SMD is around 65 micron at nearly all radial and axial locations suggesting a near uniform dispersion due to high swirl. The number density on the other hand show significant radial variations with a drop in the number density near the centerline. This may be an instantaneous artifact of the high swirl and needs to be addressed later when more time-averaged data becomes available.

6 CONCLUSIONS

This paper has reported on the application of LES to turbulent premixed combustion, fuel/air mixing and turbulent sprays in a gas turbine combustor that is a close approximation of a lean premixed combustor under development at General Electric Aircraft Engine Company. The eventual goal of this ongoing study is to develop a computational tool that can be used to investigate unsteady combustion in full-scale gas turbine combustors. As the first step toward achieving this eventual goal, the present study was focussed on evaluating the capability of LES methodologies that employ conventional subgrid mixing models. The LES methodology has been used to predict with reasonable accuracy premixed combustion in the LM-6000 using a new flame broadened model. The same LES code has been used to determine whether it can capture the experimentally observed phenomenon that the swirling fuel/air mixture generated by the dual annular counter-rotating premixer has significant spatial variation in the local equivalence ratio in the near field. This unmixedness can impact the emission characteristics of the combustor. Finally, droplet dispersion in the same type of flow field has been studied using very high grid resolution. Preliminary results indicate reasonable agreement with past observations; however, additional data is needed before making further conclusions.

An important observation from these studies is that provided advanced subgrid closure models are used in the LES coarse grid simulations can provide results with acceptable accuracy. It was also determined that these LES can be completed in matter of days (5-6) using currently available massively parallel machines. This suggests that in the near future (taking into account the expected speedup of the next generation systems), LES studies for design of full-scale combustors using 0.5-2 million grid points could be accomplished within 1-2 days. Such a quick turnaround is what is mandated by industry for design studies.

7 Acknowledgments

This work was supported in part by Air Force Office of Scientific Research under a Focussed Research Initiative (monitored by General Electric Aircraft Engine Company, Cincinnati, OH) and by the Army Research Office under a Multidisciplinary University Research Initiative. Computational support was provided by the DOD High Performance Computing Centers at NAVOCEANO, MS and ASC, WPAFB,

OH under a DOD Wright Patterson AFB Grand Challenge Project.

References

[1] Kim, W.-W. and Menon, S., "A new incompressible solver for large-eddy simulations," *International Journal of Numerical Fluid Mechanics*, Vol. to appear, 1999a.

[2] Frazier, T. R., Foglesong, R. E., Coverdill, R. E., Peters, J. E., and Lucht, R. P., "An Experimental Investigation of Fuel/Air Mixing in an Optically Accessible Axial Premixer," *AIAA-98-3543*, 1998.

[3] Fric, T. F., "Effects of Fuel-Air Unmixedness on NOx Emissions," *Journal of Propulsion and Power*, Vol. 9, No. 5, 1993, pp. 708–713.

[4] Shih, W. P., Lee, J. G., and Santavicca, D. A., "Stability and Emissions Characteristics of a Lean Premixed Gas Turbine Combustor," *Twenty-Sixth Symposium (International) on Combustion*, 1996.

[5] Menon, S. and Calhoon, W., "Subgrid Mixing and Molecular Transport Modeling for Large-Eddy Simulations of Turbulent Reacting Flows," *Twenty-Sixth Symposium (International) on Combustion*, 1996, pp. 59–66.

[6] Calhoon, W. H. and Menon, S., "Linear-Eddy Subgrid Model for Reacting Large-Eddy Simulations: Heat Release Effects," *AIAA-97-0368*, 1997.

[7] Smith, T. M. and Menon, S., "Subgrid Combustion Modeling for Premixed Turbulent Reacting Flows," *AIAA-98-0242*, 1998.

[8] Menon, S., Pannala, S., Kim, W.-W., Chakravarthy, V. K., and Henry, W., "Numerical Simulations of Turbulent Reacting Sprays," *HPC DOD Users Group Meeting*, 1999.

[9] Erlebacher, G., Hussaini, M. Y., Speziale, C. G., and Zang, T. A., "Toward the Large-Eddy Simulation of Compressible Turbulent Flows," *Journal of Fluid Mechanics*, Vol. 238, 1992, pp. 155–185.

[10] Menon, S. and Pannala, S., "Subgrid modeling of unsteady two-phase turbulent flows," *AIAA Paper No. 97-3113*, 1997.

[11] Faeth, G. M., "Evaporation and combustion of sprays," *Progress in Energy and Combustion Science*, Vol. 9, 1983, pp. 1–76.

[12] Oefelein, J. C. and Yang, V., "Analysis of transcritical spray phenomena in turbulent mixing layers," *AIAA 96-0085, 34th AIAA Aerospace Sciences Meeting*, 1996.

[13] Pannala, S. and Menon, S., "Large eddy simulations of two-phase turbulent flows," *AIAA 98-0163, 36th AIAA Aerospace Sciences Meeting*, 1998.

[14] Kim, W.-W. and Menon, S., "A New Dynamic One-Equation Subgrid-Scale Model for Large-Eddy Simulations," *AIAA-95-0356*, 1995.

[15] Menon, S., Yeung, P.-K., and Kim, W.-W., "Effect of Subgrid Models on the Computed Interscale Energy Transfer in Isotropic Turbulence," *Computers and Fluids*, Vol. 25, No. 2, 1996, pp. 165–180.

[16] Kim, W.-W., Menon, S., and Mongia, H. C., "Large-Eddy Simulation of a Gas Turbine Combustor Flow," *Combustion Science and Technology* (to appear).

[17] Germano, M., Piomelli, U., Moin, P., and Cabot, W. H., "A Dynamic Subgrid-Scale Eddy viscosity Model," *Physics of Fluids A*, Vol. 3, No. 11, 1991, pp. 1760–1765.

[18] Cabot, W. H. and Moin, P., "Large Eddy Simulation of Scalar Transport with the Dynamic Subgrid-Scale Model," *LES of Complex Engineering and Geophysical Flows*, edited by B. Galperin and S. Orszag, Cambridge University Press, 1993, pp. 141–158.

[19] Lund, T. S., Ghosal, S., and Moin, P., "Numerical Experiments with Highly-Variable Eddy Viscosity Models," *Engineering Applications of Large Eddy Simulations*, edited by U. Piomelli and S. Ragab, Vol. 162 of *FED*, ASME, 1993, pp. 7–11.

[20] Wong, V. C., "A Proposed Statistical-Dynamic Closure Method for the Linear or Nonlinear Subgrid-Scale Stresses," *Physics of Fluids A*, Vol. 4, No. 5, 1992, pp. 1080–1082.

[21] Fureby, C., "Towards Large Eddy Simulations of Flows in Complex Geometries," *AIAA-98-2806*, 1998.

[22] Fureby, C., Tabor, G., Weller, H. G., and Gosman, A. D., "A Comparative Study of Subgrid Scale Models in Homogeneous Isotropic Turbulence," *Physics of Fluids*, Vol. 9, No. 5, 1997, pp. 1416–1429.

[23] Frankel, S. H., Adumitroaie, V., Madnia, C. K., and Givi, P., "Large Eddy Simulation of Turbulent Reacting Flows by Assumed pdf Methods," *Engineering Applications of Large Eddy Simulations*, edited by U. Piomelli and S. Ragab, Vol. 162 of *FED*, ASME, 1993, pp. 81–101.

[24] Menon, S., McMurtry, P., and Kerstein, A. R., "A Linear Eddy Mixing Model for Large Eddy Simulation of Turbulent Combustion," *LES of Complex Engineering and Geophysical Flows*, edited by B. Galperin and S. Orszag, Cambridge University Press, 1993.

[25] Kim, W.-W. and Menon, S., "Numerical Modeling of Fuel/Air Mixing in a Dry Low-Emission Premixer," Second AFOSR International Conference on DNS and LES, Rutgers University, June 7-9, 1999 (to be presented).

[26] Smith, T. M., *Unsteady Simulations of Turbulent Premixed Reacting Flows*, Ph.D. thesis, Georgia Institute of Technology, Atlanta, GA, March 1998.

[27] Yakhot, V., "Propagation Velocity of Premixed Turbulent Flames," *Combustion Science and Technology*, Vol. 60, 1988, pp. 191–214.

[28] Pocheau, A., "Scale Invariance in Turbulent Flont Propagation," *Physical Review E*, Vol. 49, 1994, pp. 1109–1122.

[29] Ashurst, W., Kerstein, A., Kerr, R., and Gibson, C., "Alignment of vorticity and scalar gradient with strain rate in simulated Navier-Stokes turbulence," *Physics of Fluids A*, Vol. 30, No. 8, 1987, pp. 2343–2353.

[30] Kim, W.-W. and Menon, S., "Large-Eddy Simulations of Turbulent Premixed Flames in the Thin Reaction Zone Regime," *AIAA-99-2816*, 1999.

[31] Ronney, P. D. and Yakhot, V., "Flame Broadening Effects on Premixed Turbulent Flame Speed," *Combustion Science and Technology*, Vol. 86, 1992, pp. 31–43.

[32] Menon, S. and Pannala, S., "Subgrid combustion simulations of reacting two-phase shear layers," *AIAA Paper No. 98-3318 ,34th AIAA/ASME/SAE/ASEE Joint Propulsion Conference and Exhibit*, 1998.

[33] Joshi, N. D., Mongia, H. C., Leonard, G., Stegmaier, J. W., and Vickers, E. C., "Dry Low Emissions Combustor Development," *ASME-98-GT-310*, 1998.

[34] Kim, W.-W. and Menon, S., "LES of Turbulent Fuel/Air Mixing in a Swirling Combustor," *AIAA-99-0200*, 1999.

[35] Poinsot, T., Echekki, T., and Mungal, M. G., "A Study of the Laminar Flame Tip and Implications for Premixed Turbulent Combustion," *Combustion Science and Technology*, Vol. 81, 1992, pp. 45–73.

[36] Cheng, R. K., "Velocity and Scalar Characteristics of Premixed Turbulent Flames stabilized by Weak Swirl," *Combustion and Flame*, Vol. 101, 1995, pp. 1–14.

[37] Peters, N., "Laminar Flamelet Concepts in Turbulent Combustion," *Twenty-First Symposium (International) on Combustion*, 1986, pp. 1231–1250.

[38] Peters, N., "Propagating Thin Reaction Zones in Premixed Turbulent Combustion. Part I: Theory and Modelling Aspects," (submitted).

[39] Chakravarthy, V. and Menon, S., "Large-Eddy simulations of bluff body stabilized flames," *Proceedings of FEDSM'99 3rd ASME/JSME Joint Fluids Engineering conference*, 1999.

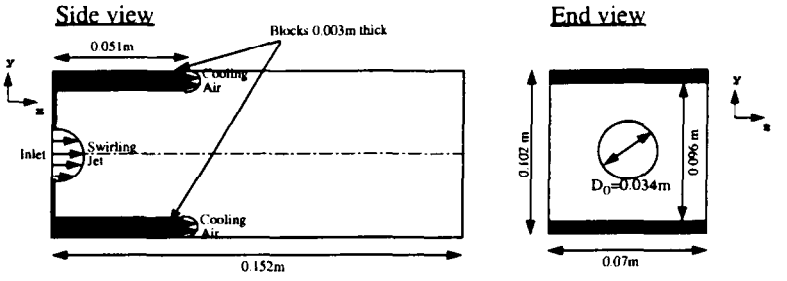

Fig. 1 Schematic of the LM-6000 being tested at General Electric

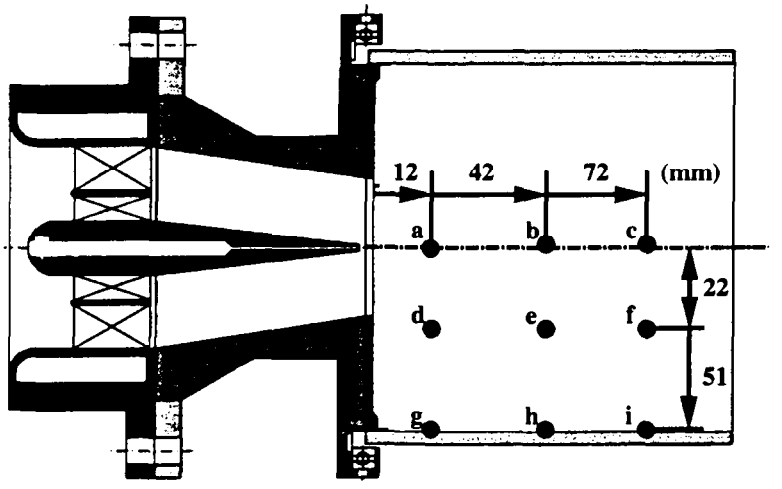

Fig. 2 Schematic of the combustor being studied at University of Illinois, UC to investigate fuel-air mixing

Fig. 3 Prediction of the flame structure using the flame broadening correction to the Yakhot's model and the dynamic closure of the G-equation.

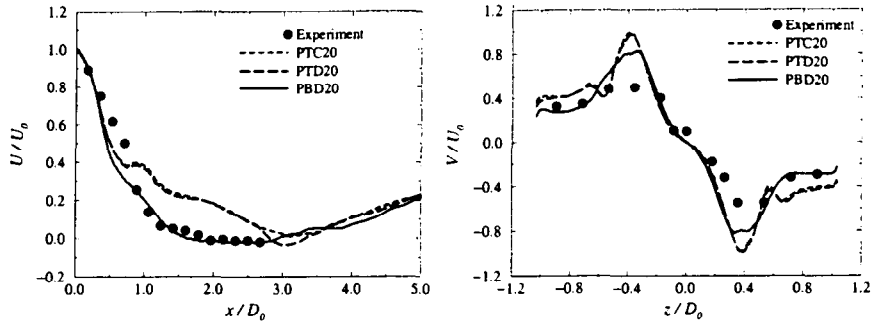

a) Centerline mean axial velocity b) Mean Tangential velocity

Fig. 4 Prediction of the mean velocity profiles in the LM-6000 at $x/D_0 = 0.18$

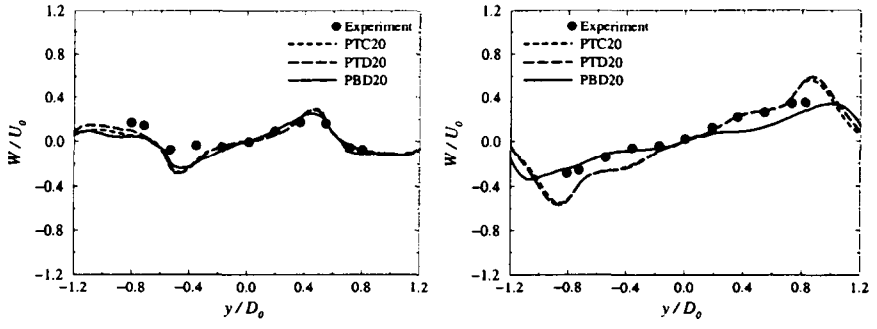

a) $x/D_0 = 0.18$ b) $x/D_0 = 0.72$

Fig. 5 Prediction of the mean radial velocity profiles in the LM-6000

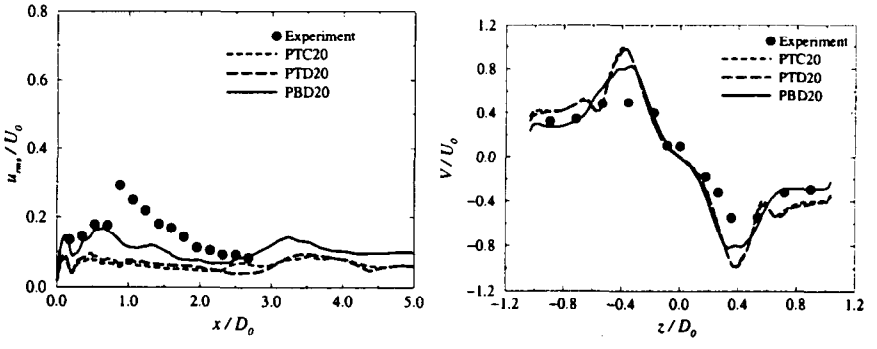

a) $y/D_0 = z/D_0 = 0$ (Centerline) b) $y/D_0 = z/D_0 = 0.81$

Fig. 6 Prediction of the axial velocity fluctuations in the axial direction

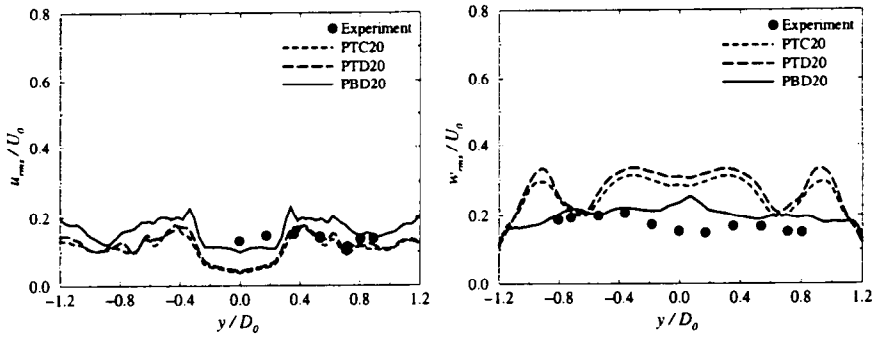

a) u_{rms} at $x/D_0 = 0.18$ b) w_{rms} at $x/D_0 = 0.72$

Fig. 7 Prediction of the velocity fluctuations at different axial locations

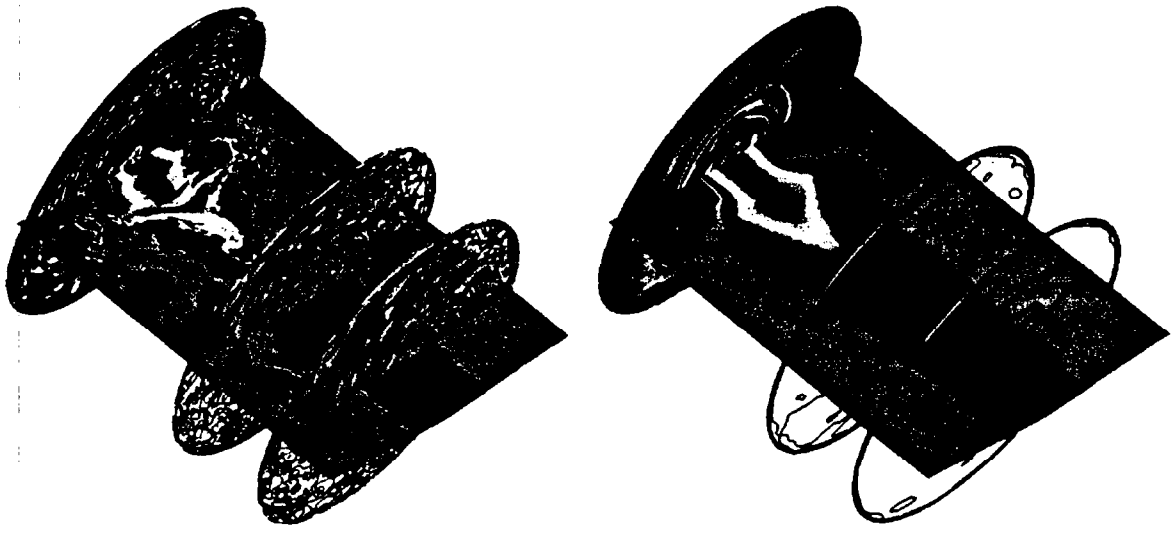

a) Instantaneous flow field b) Time-averaged flow field

Fig. 8 Comparison of instantaneous flow field and time-averaged data in the UIUC combustor. The circular planes show that vorticity magnitude in three axial planes and the spanwise plane shows the fuel species distribution. Clearly, time-averaging smoothes all the finer details seen in the instantaneous flow field and gives a misleading picture.

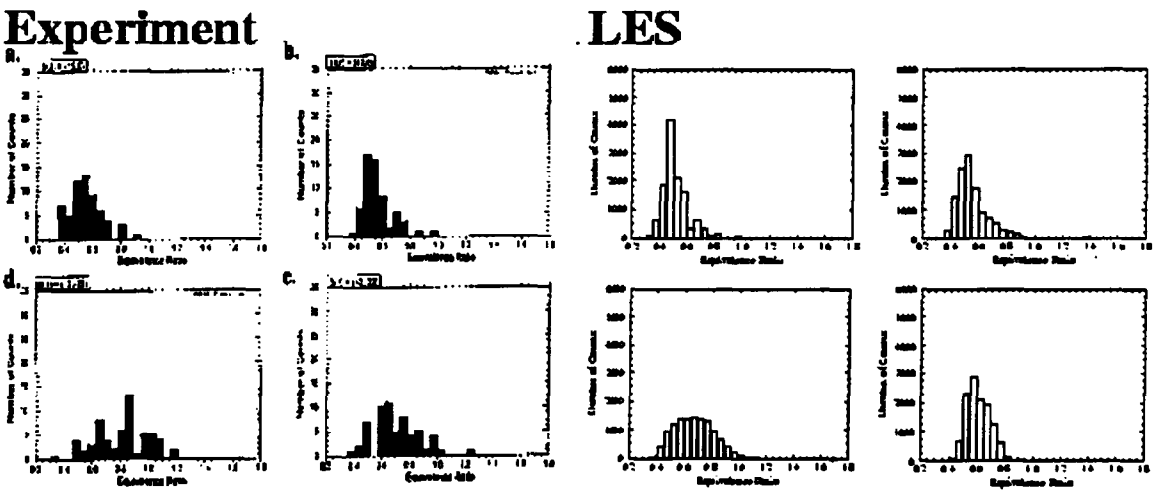

Fig. 9 Comparison of the histograms obtained from the experiments and the LES. Note that, experimental data was obtained from only 60 samples which is considered insufficient for statistical analysis.

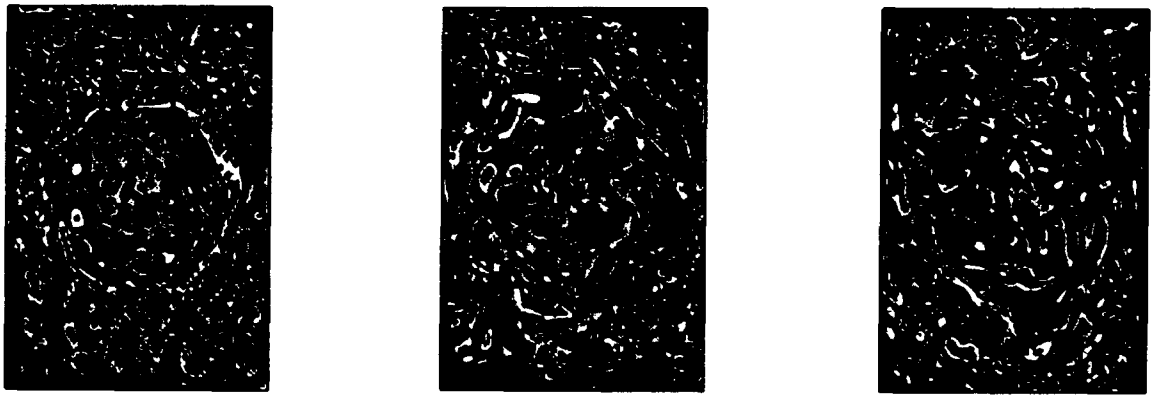

a) $x/D = 0.10$ b) $x/D = 0.25$ c) $x/D = 0.50$

Fig. 10 Instantaneous vorticity contours and droplet distribution at various axial locations

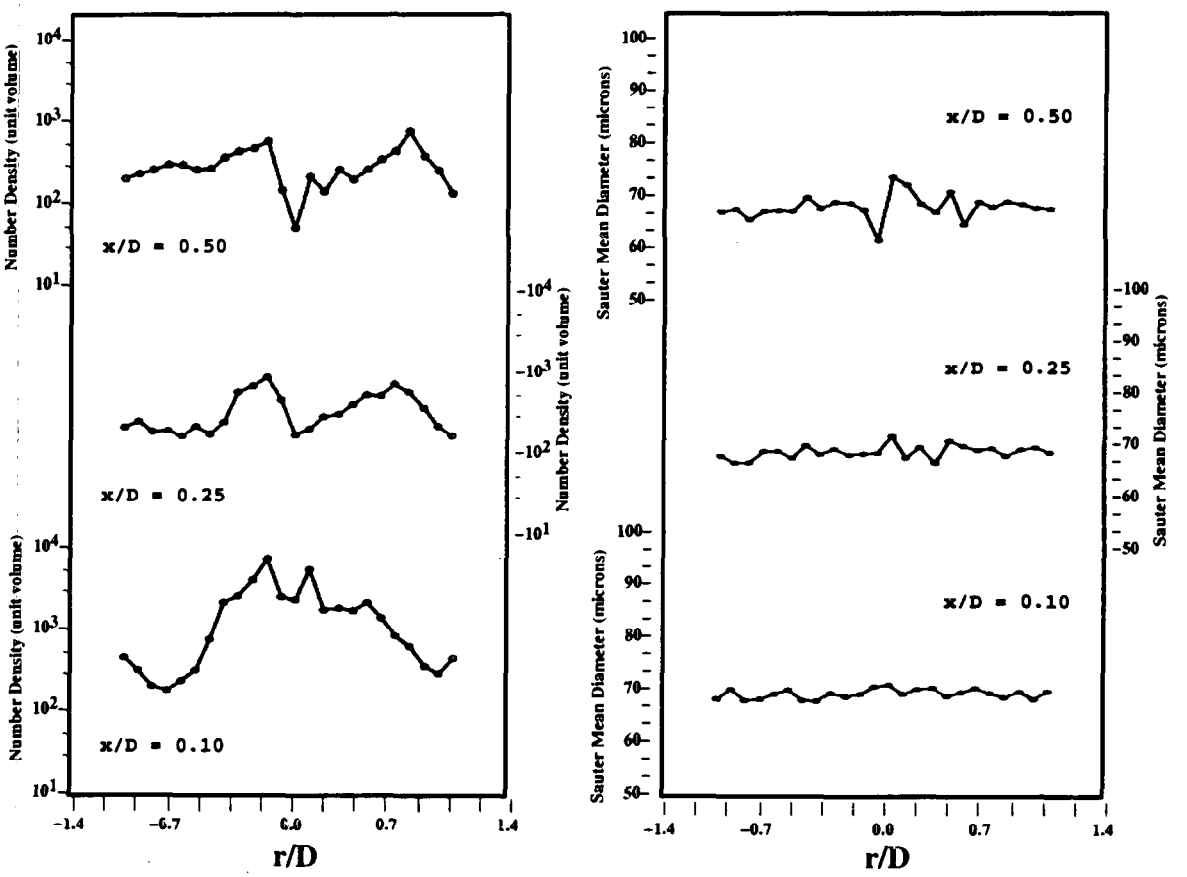

a) Number Density

b) Sauter Mean Diameter

Fig. 11 Droplet number density and Sauter Mean diameter at various axial locations